Physics and Chemistry of Minerals (2022) 49:10
https://doi.org/10.1007/s00269-022-01185-7

ORIGINAL PAPER

A chondrule formation experiment aboard the ISS: microtomography, scanning electron microscopy and Raman spectroscopy on Mg_2SiO_4 dust aggregates

Dominik Spahr[1] · Tamara E. Koch[1] · David Merges[1] · Lkhamsuren Bayarjargal[1] · Philomena-Theresa Genzel[1] · Oliver Christ[1] · Fabian Wilde[2] · Frank E. Brenker[1] · Björn Winkler[1]

Received: 17 September 2021 / Accepted: 8 January 2022 / Published online: 3 May 2022

Abstract

We performed an experiment under long-term microgravity conditions aboard the International Space Station (ISS) to obtain information on the energetics and experimental constraints required for the formation of chondrules in the solar nebula by 'nebular lightning'. As a simplified model system, we exposed porous forsterite (Mg_2SiO_4) dust particles to high-energetic arc discharges. The characterization of the samples after their return by synchrotron microtomography and scanning electron microscopy revealed that aggregates had formed, consisting of several fused Mg_2SiO_4 particles. The partial melting and fusing of Mg_2SiO_4 dust particles under microgravity conditions leads to a strong reduction of their porosity. The experimental outcomes vary strongly in their appearance from small spherical melt-droplets (∅ ≈ 90 µm) to bigger and irregularly shaped aggregates (∅ ≈ 350 µm). Our results provided new constraints with respect to energetic aspects of chondrule formation and a roadmap for future and more complex experiments on Earth and in microgravity conditions.

Keywords Microgravity · Arc discharges · International Space Station ISS · Chondrule formation · Microtomography

Introduction

Experiments performed under extreme conditions such as high pressures or high temperatures have been carried out in very large number during the last decades leading to a better understanding of, e.g. physical properties of minerals or phase relations. Another much less explored extreme condition is microgravity, which can be achieved by parabolic flights, drop-tower experiments or outside the Earth's atmosphere. Currently, long-term microgravity is only available outside the Earth's atmosphere, either aboard the International Space Station (ISS) or using other satellite-based experimental platforms. As commercial payloads for the ISS were made accessible for researchers, we developed the first chondrule formation experiment, which was carried out in long-term microgravity aboard the ISS, with the acronym EXCISS (**Ex**perimental **C**hondrule formation aboard the **ISS**) (Spahr et al. 2020).

Chondrules have been considered to be the building blocks of our solar system in most of the models for planet and planetesimal formation, but their formation process is debated controversially (Russel et al. 2018; Boss 1996; Kerr 2013; Connolly and Jones 2016). Different scenarios for chondrule formation have been proposed, for example formation by shock waves (Connolly and Love 1998; Ciesla and Hood 2002), by nebular lightnings (Whipple 1966; Horányi et al. 1995; Desch and Cuzzi 2000; Túnyi et al. 2003; Güttler et al. 2008; Johansen and Okuzumi 2018) or by collisions of planetesimals (Krot et al. 2005; Asphaug et al. 2011; Johnson et al. 2015; Lichtenberg et al. 2018). Since there is no single theory which can explain all chondrule characteristics, different events could contribute to chondrule formation (Morris and Boley 2018).

This article is part of a Topical Collection "Experimental & Analytical Techniques at Extreme & Ambient Conditions", guest edited by Stella Chariton, Vitali B. Prakapenka and Haozhe (Arthur) Liu.

✉ Dominik Spahr
d.spahr@kristall.uni-frankfurt.de

[1] Institute of Geosciences, Goethe University Frankfurt, Altenhöferallee 1, 60438 Frankfurt, Germany

[2] Institute of Materials Physics, Helmholtz-Zentrum Hereon, Max-Planck-Straße 1, 21502 Geesthacht, Germany

Experiments can help to test proposed formation conditions and mechanism, but previous chondrule formation experiments only partially successfully reproduced properties of chondrules as they were affected by the gravity on Earth (Wdowiak 1996; Lofgren 1996; Connolly et al. 1998; Hewins et al. 2000; Hewins and Fox 2004; Güttler et al. 2008; Morlok et al. 2012; Imae and Isobe 2017). Therefore, we developed the EXCISS experiment which was focused on the chondrule formation by 'nebular lightning'. The long-term microgravity conditions aboard the ISS enable us to expose the Mg_2SiO_4 particles to arc discharges without the influence of gravity. The hypothesis of chondrule formation by nebular lightnings was recently supported by, e. g. Johansen and Okuzumi (2018). This study provided evidence that the decay of short-lived ^{26}Al ($\tau = 7 \times 10^5$ years) may lead to the charging of dust particles in the solar nebular with subsequent discharges through lightning bolts. This finding implies that lightnings can provide enough energy to melt mm-sized particles, which is one of the main uncertainties of the nebular lightning theory. The fast cooling rates assumed for the thermal history of chondrules formed by 'nebular lightning' contradict the previously expected cooling rates for the formation of the most common chondrules. However, Libourel and Portail (2018) presented new constraints on chondrule formation and their thermal history, which may be consistent with cooling rates up to 10^6 K h^{-1}.

In the EXCISS experiment, freely floating forsterite (Mg_2SiO_4) dust particles were exposed to high energetic arc discharges which can reach electron temperatures up to $k_B T_e \approx 6900$ K (Spahr et al. 2020). We chose Mg_2SiO_4 as a model system for our experiments as it is the most abundant phase in natural chondrules and has a relatively high melting point of ≈ 2200 K (Russel et al. 2018; Bowen and Schairer 1925). The experiments were observed by a camera and the sample material was analyzed after sample return. The analysis of the video material revealed the particle behavior of agitated particles in electric field in long-term microgravity environment (Koch et al. 2021a). In this study, we have shown that the electric fields influence the aggregation process, the aggregate morphology and the internal structure. These observations can help to understand different aggregation processes in the early Solar System. The experiment also caused the formation of fused aggregates and melt spherules. In our investigations on the small spherical melt droplets, we have shown that the sample material can be completely melted by arc discharges into melt spherules (Koch et al. 2021b). The analysis of these droplets with scanning electron microscopy and electron-back-scattered diffraction showed, that the micro-textural properties of these spherules, such as crystal sizes and orientations, morphologies and metal inclusions, are very similar to those observed in natural chondrules. The microstructure is probably the result of crystallization under microgravity conditions. In addition, the fused aggregates show similarities to different types of Ca,Al-rich inclusions, the oldest material of our Solar System (Koch et al. 2022). These results imply that a (flash-)heating event with subsequent aggregation could have been involved in the formation of different morphological CAI-characteristics.

In the study presented here we investigated the behavior of Mg_2SiO_4 dust particles exposed to high energetic electrical discharges under long-term microgravity conditions. In contrast to the test experiments on Earth (Spahr et al. 2020) the Mg_2SiO_4 particles levitated without gravitational influence in the sample chamber during the whole experimental procedure aboard the ISS. Mg_2SiO_4 dust particles or already formed aggregates may then be exposed to multiple discharges, which was not possible in the test experiments. We used synchrotron based X-ray microtomography as a tool to study the density contrast in fused dust aggregates and melt-droplets received from experiments aboard the ISS after sample return. Furthermore, we visualized their inner structures and grain-grain boundaries. The microtomography data were complemented by high-resolution scanning electron microscopy images and the phase content was studied by Raman spectroscopy.

Materials and experimental methods

Sample material

The initial Mg_2SiO_4 pellets were obtained by high-temperature synthesis using pressed pellets of the oxides as starting material, resulting in a sintered Mg_2SiO_4 ceramic. The pellets were then ground in an agate mortar and sieved. The chemical composition and the phase purity of the resulting powder was confirmed by scanning electron microscopy and Rietveld refinement on the X-ray powder diffraction data, respectively. The Mg_2SiO_4 particles selected after the grinding by sieving had a mean diameter of 126(23) µm and hence can easily be observed by the microscope camera in the experimental setup (Spahr et al. 2020). The high porosity of the initial dust particles allows to unambiguously determine if a melting process took place and which amount of the initial grains was molten. After sample return from the ISS the sample chamber was opened and Mg_2SiO_4 dust aggregates and melt-droplets were hand-picked from the received powder and sorted under a microscope.

Experiments aboard the ISS

The experimental setup and its calibration is described in Spahr et al. (2020) in great detail. The experiment was carried out inside a $10 \times 10 \times 15$ cm^3 sized NanoRacks NanoLab aboard the ISS. The Mg_2SiO_4 dust particles were

freely levitating inside a glass sample chamber while they were exposed to high energetic electrical discharges with an adjustable energy between 3.1 J and 21 J. The sample chamber was made of quartz glass and we used tungsten electrodes with a diameter of 1 mm and a spark gap of ≈ 2–3 mm for the discharges. The chamber was loaded with 30(1) mg of the Mg_2SiO_4 powder and the argon gas pressure inside the chamber was adjusted to be 100(1) mbar. The arc discharges between the W-electrodes can have a duration between 400 and 600 µs and reach electron temperatures up to $k_B T_e \approx 6900$ K with electron densities up to $n_e \approx 2 \times 10^{16}$ cm^{-3}. The changes in particle size and morphology after the discharges were recorded with a Raspberry Pi camera. Figure 1 shows frames recorded with a high-speed camera of a typical arc discharge in the sample chamber during the test experiments on Earth. The first frame shows the weak ignition spark. The time interval between the frames is 20 µs. The released energy during this arc discharge was ≈ 8 J.

Aboard the ISS the EXCISS experiment was operated for 30 days. It was connected by USB to the ISS for power supply and data transfer. During this time the initial Mg_2SiO_4 dust particles in the sample chamber were exposed to 81 arc discharges. Based on our previous calibration the estimated energy of the released arc discharges was between 5 J and 8 J. Figure 2 shows the field of view in the sample chamber aboard the ISS after 30 arc discharges. The light transmission through the sample chamber is reduced due to the formation of a thin film of tungsten, deposited on the inner glass surface after being sputtered from the electrodes. The aggregates, which were freely levitating in microgravity and later found on the bottom of the sample chamber without sticking to the inner walls or electrodes, were used for the subsequent microtomography, SEM and Raman analysis. The tips of the electrodes are eroded by the arc discharges.

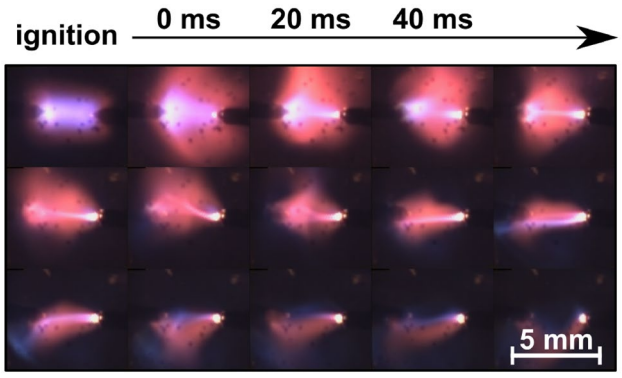

Fig. 1 High-speed photographs of an arc discharge where ≈ 8 J are released into the spark gap. The first picture shows the weak ignition spark. The time interval between the frames is 20 µs

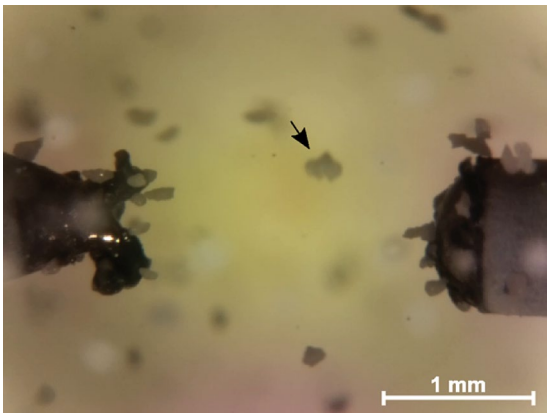

Fig. 2 Field of view aboard the ISS after 30 arc discharges. Bigger agglomerated objects stick to the electrodes and are levitating in between

Synchrotron microtomography

Synchrotron microtomography was performed on the microtomography beamline P05 (Wilde et al. 2016; Ogurreck et al. 2013), operated by Helmholtz-Zentrum Geesthacht at PETRA III (DESY) in Hamburg, Germany. All data were collected using a 15 keV beam and the double crystal monochromator. The high quality absorption contrast tomograms were acquired using a 24× objective lens with a CMOS camera resulting in a 1.8×1.8 mm^2 field of view. A $CdWO_4$ single crystal scintillator with 100 µm thickness was employed for the X-ray to visible light conversion. We used an acquisition time of 350 ms per frame. A binning factor of 2×2 pixel resulted in a binned pixel size of ≈ 0.61×0.61 µm^2 and the spatial resolution was estimated to be 1 µm. Data pre-processing, including tomographic reconstruction was performed using MATLAB scripts provided by Moosmann et al. (2014). The microtomography reconstructions were visualized with the volume exploration software tool Drishti (Limaye 2012). The samples were embedded in Araldite epoxy resin and afterwards dried at 333 K under vacuum for 24 hours to ensure their stability during transport and measurement. The high density contrast between the Araldite epoxy ($\rho \approx 1$ g cm^{-1}) and the forsterite ($\rho \approx 3.3$ g cm^{-1}) prevented a deterioration of the tomographic reconstruction of the embedded aggregates. All objects were embedded and measured individually.

Scanning electron microscopy

We used a Phenom World ProX desktop SEM equipped with an back-scattered Electron detector (BSE) for scanning electron microscopy (SEM). The samples were used as received and mounted without coating using sticky carbon tape on aluminum stubs. They were measured under low vacuum

conditions to reduce charging effects on the sample with 10 kV for imaging. We used the software Helicon Focus 7 Pro (Kozub et al. 2018) from Helicon Soft to combine multiple BSE images acquired with different focal planes to obtain images with an improved depth of field. We used the depth map rendering method with radius = 8 (size of the analyzed area around each pixel) and smoothing = 4 (value determines how depth map will be smoothed out). Energy-dispersive X-ray spectroscopy (EDX) was carried out using 15 kV and the obtained data were analyzed using the Phenom Pro Suite software.

Raman spectroscopy

Raman spectroscopy was performed using an OXXIUS S.A. LaserBoxx LMX532 laser ($\lambda = 532.14$ nm) in combination with a Pixis256E CCD camera mounted on a Princeton Instruments ACTON SpectraPro 2300i spectrograph. The Raman setup is described in Bayarjargal et al. (2018) in more detail and the Raman spectra were background corrected using the software Fityk (Wojdyr 2010).

Results

Starting material

The Mg_2SiO_4 dust particles which were used as starting material for the ISS-based experiment had a mean diameter of 126(23) µm (Fig. 3a). The SEM and synchrotron microtomography images (Fig. 3) show that they were irregularly shaped and have rough surfaces. In addition, the microtomography reconstruction also shows a homogeneous density distribution inside the grains confirming the structural and chemical homogeneity of the starting material (Fig. 3b). The high porosity of the dust particles can also be observed which is in good agreement with our earlier investigations (Spahr et al. 2020). In addition, the expected chemical composition was confirmed by EDX analysis within the experimental uncertainties and no unexpected elements were detected.

Aggregates formed aboard the ISS

Synchrotron microtomography

Aboard the ISS we successfully melted Mg_2SiO_4 dust particles or fused them together to bigger objects. We used synchrotron microtomography as a tool to study their inner structure and density distribution. After the sample return, the samples display a morphological diversity as we obtained small and spherical melt-droplets (Fig. 4) and fused aggregates which can have many different shapes (Fig. 5). The spherical objects or melt-droplets (≈ 90 µm) have a smooth surface and a strongly reduced porosity in comparison to the initial dust particles (Fig. 3). The melt-droplets must have been melted by the lightnings induced in the experiment and afterwards cooled down without gravitational influence. The melt-droplet (Fig. 4) shows a region with strongly increased density (orange). This is probably caused by an impact of a very hot tungsten particle from the electrode. Other parts of the melt-droplet show a lower density, which can be explained by unmolten regions with pores. The scale bar of the reconstructed absorption contrast tomograms was adjusted to show only objects with a density larger than the surrounding Araldite epoxy resin. Hence, the 3D-reconstruction of the surface of the particles and aggregates is assumed to be the area where the density is higher than the epoxy.

We found by SEM and EBSD analysis in a related study (Koch et al. 2021b) that microtextural properties of the melt-droplets partially resemble those of natural chondrules, e.g. with respect to crystal sizes, crystal orientations, or morphologies. They seem to have a texture comparable to porphyritic chondrules which is the most abundant chondrule type (Russell et al. 2018). Very recent studies reveal that

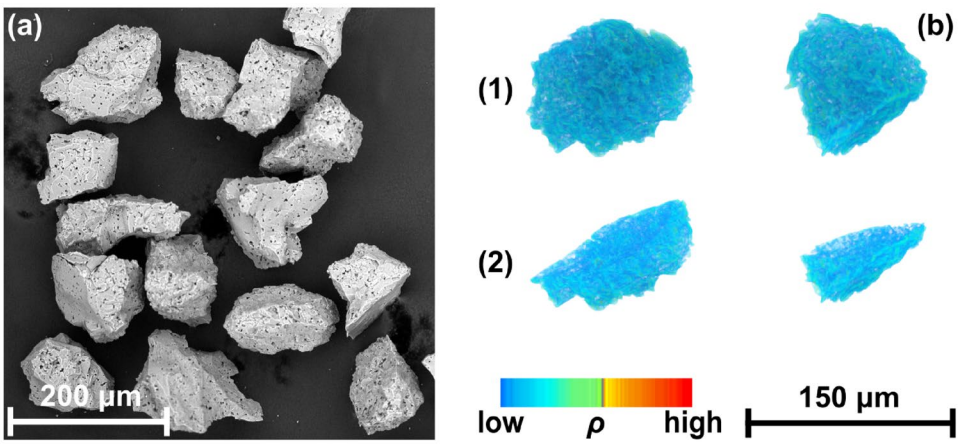

Fig. 3 **a** SEM image of different Mg_2SiO_4 particles after the sample preparation process. **b** Synchrotron microtomography on representative Mg_2SiO_4 dust particles with a 3D-reconstruction of the surface (1) and virtual cross-section through the grains (2)

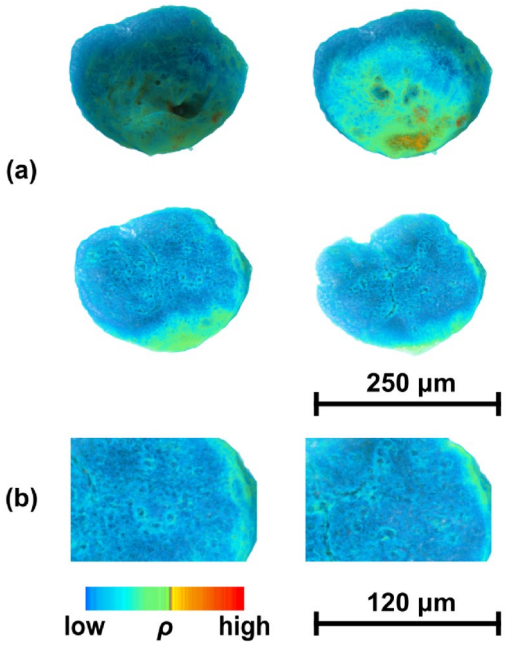

Fig. 4 Synchrotron microtomography image of a spherical melt-droplet formed aboard the ISS: **a** 3D-reconstruction of the surface (left top) and three virtual cross-sections through the same melt-droplet. **b** Close-ups of selected regions in the cross-sections

porphyritic textured chondrules may be obtained by experiments with very high cooling rates (3000–6000 K h^{-1}) (Greenwood and Herbst 2021), in agreement with the very fast cooling rates in our discharge experiment. A columnar crystal morphology was observed in some parts of the melt-droplets (Koch et al. 2021b) which has also been observed in natural porphyritic chondrules (Libourel and Portail 2018). However, due to the use of a the single phase Mg_2SiO_4 starting material, the glassy mesostasis typical for porphyritic chondrules was not observed in our experiments.

The size of the melt droplets is significantly smaller than from the fused dust aggregates formed of several Mg_2SiO_4 grains. Their size ranges from ≈ 150–350 µm depending on the number of participating Mg_2SiO_4 dust grains and on their shape. Figure 5 shows four representative aggregates. Aggregate #1 consists of 2–3 Mg_2SiO_4 dust particles. Half of this aggregate was completely molten and shows an increased density while in the rest of the aggregate regions with low density and high porosity can be identified. The very high density (orange) is probably caused by the impact of a hot/molten tungsten particle from the electrodes. Other aggregates consist of more initial dust particles. Aggregate #2 is much bigger with ≈ 350 µm diameter. This aggregate is still irregularly shaped but molten areas on the surface can clearly be identified. Furthermore, the virtual cross-section through the

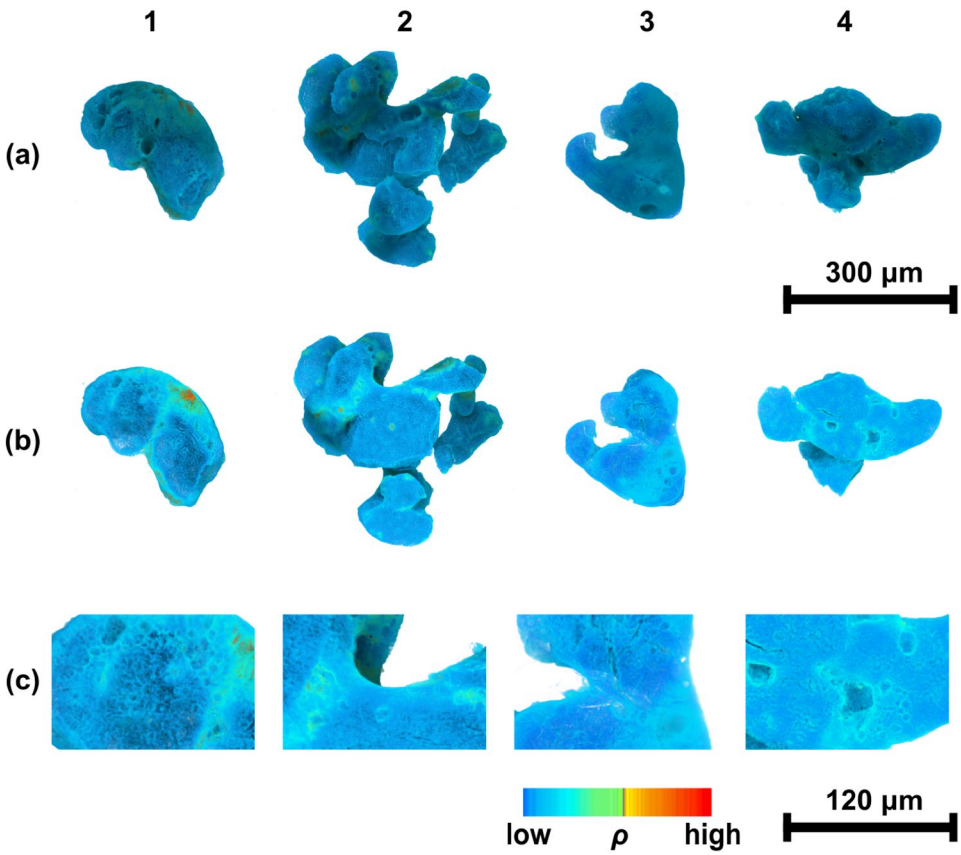

Fig. 5 Synchrotron microtomography images of differently shaped and sized aggregates #1–4 formed aboard the ISS (**a**), corresponding virtual cross-sections (**b**) and close-ups of selected regions in the cross-sections (**c**)

aggregate clearly shows an increased density (green) on the grain boundaries of the former dust particles which corresponds to molten regions. In this area, the high porosity of the starting material has disappeared. Small regions with very high density (orange) indicate tungsten contamination from the electrodes.

Aggregate #3 is not completely spherically shaped but has the shape of a hemisphere. The whole surface is smooth and rounded, which indicates that the surface was completely molten. In the surface reconstruction (a) the initial Mg_2SiO_4 dust particles cannot be identified any more. However, the virtual cross-section (b) shows that the inner part in the upper region is still unmolten while the bottom part of the aggregate was molten. In addition, larger pores grow during the melting process. Enlarged pores can also be observed in the cross-section of aggregate #4. These pores were surrounded by molten regions with higher (green) density. In the surface reconstruction of aggregate #4 the increased density can also be observed in the region where the former Mg_2SiO_4 melted together, but here the initial Mg_2SiO_4 can still be identified. These observations are in good agreement with our test experiments on Earth (Spahr et al. 2020) were we observed increased density on the contact points between grains or in the regions where tungsten from the electrodes impacts into Mg_2SiO_4 grains.

The relatively small differences in the density contrast (Fig. 5 aggregates #2–#4) are caused by the homogeneous chemical composition of the starting material. This confirms that the fused aggregates were chemically uniform and not formed e. g. around hot tungsten particles as observed for aggregate #1 or during the Earth based experiments (Spahr et al. 2020). Small changes in the contrast only occur due to a slightly increased density in the molten regions, confirming that the aggregates were formed in the arc discharge and not by the impact of hot tungsten particles. The role of a small amount of tungsten vapor from the electrodes, which cannot be detected by microtomography, during the melting and fusing process of the aggregates is unknown.

Scanning electron microscopy

We used scanning electron microscopy to obtain high-resolution images of the surfaces of the fused aggregates (Fig. 6). With lower magnification (a) the initial Mg_2SiO_4 dust particles can be identified in some regions of the aggregates, but it is obvious that the dimensions of the dust aggregates formed during the experiment (up to 400 µm) are much bigger than of the starting material.

Aggregate #5 is elongated in one direction and in the outer part the Mg_2SiO_4 dust particles seem to be pristine. In contrast to the enlarged part in the center of the aggregate where a large amount of melt covers at least the surface of one or two Mg_2SiO_4 grains and connects them to the surrounding particles. The surface of aggregate #6 is smooth and rounded in many regions. These areas of the aggregate were molten before, and in the left part of the aggregate the initial Mg_2SiO_4 grains and their contact points cannot be identified any more. Furthermore, a spherical melt-droplet is part of the aggregate. The melt-droplet connects the left and molten part with a nearly unchanged Mg_2SiO_4 grain on the opposite side. The surface of this melt-droplet varies widely from the surfaces of the other aggregates. A similar melt-droplet within an aggregate was also found in our test experiments on Earth (Spahr et al. 2020). In aggregate #7 only a few parts are molten and with increased magnification it can be observed that some regions of the initial Mg_2SiO_4 grains were completely molten and rounded while other parts of the same grain were untouched. Aggregate #7 is held together by the molten areas of a few grains which connects them to the surrounding unmolten particles. In contrast to aggregate #7, in aggregate #8 large parts of the aggregate were molten. The bottom part is covered with a coherent layer of molten material. In some parts the layer is incomplete and unveils an inside look on the unmolten bottom layer.

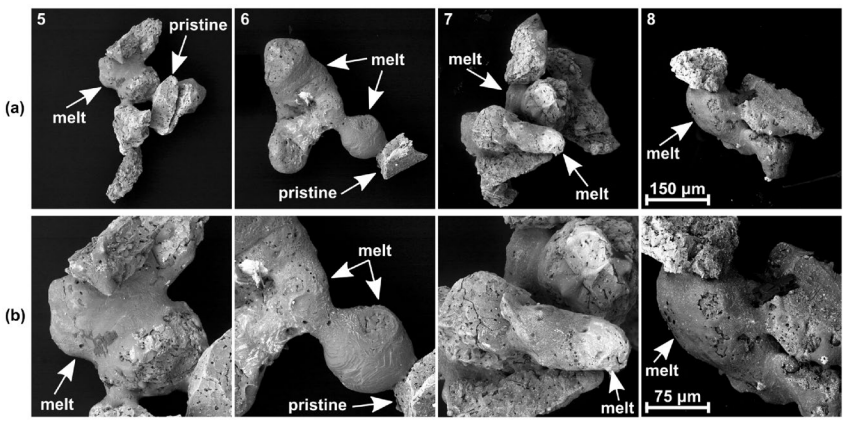

Fig. 6 SEM images of different aggregates #5–8 formed aboard the ISS with lower (**a**) and higher (**b**) magnification. Characteristic pristine and melt regions are marked

The EDX measurements on the aggregates reveal, that the expected chemical composition of the Mg_2SiO_4 dust particles does not change during the melting process. In contrast to the starting material, we found a slight tungsten contamination in some regions of the fused dust aggregates. This is in good agreement with the small regions having a very high density, observed by microtomography.

Raman spectroscopy

We used Raman spectroscopy to determine the mineral phases occurring in the dust aggregates. Figure 7 shows line measurements through selected aggregates. A picture section of the corresponding SEM image (Fig. 6b) shows the position where the Raman spectra were acquired. It is clear to see that even in the molten regions crystalline forsterite is present, the predominant phase and has not decomposed. No significant peak broadening can be observed in the molten regions and all Raman modes of the pristine areas can still be observed. Only minor peaks of an additional phase can be observed in a few Raman spectra.

Discussion and conclusion

As we successfully demonstrated that melting of Mg_2SiO_4 dust particles is possible with our experimental setup within the chosen experimental conditions, we cross-checked the required energy for melting our Mg_2SiO_4 precursor particles. The discharge energy was adjusted up to the ≈ 8 J, while below no significant changes in the particle texture or morphology had been observed with the integrated camera. After several discharges with energies between 5 J and 8 J first changes were observed in the particle texture and morphology (Fig. 2). Therefore, we chose to not further increase the energy of the arc discharge. The precursor dust particles with a diameter of $d = 0.126(23)$ mm and a density of $\rho = 3.2$ g cm^{-3} have a mass of $m_{\mathrm{dust}} \approx 2.5 \times 10^{-5}$ g approximating them as spheres. We calculated the required melting energy (Q_{melt}) for the chosen precursor material using the enthalpy of fusion ($\Delta H_{\mathrm{fus}} = 114(20)$ kJ mol^{-1}Navrotsky et al. 1989) and the molar mass ($M = 140.7$ g mol^{-1}) of Mg_2SiO_4:

$$Q_{\mathrm{melt}} = \Delta H_{\mathrm{fus}} \cdot \frac{m_{\mathrm{dust}}}{M_{\mathrm{Mg_2SiO_4}}}. \quad (1)$$

The required melting energy is ≈ 0.02 J per dust particle for a complete melting in the arc discharge. The highest energy used for the discharge experiments aboard the ISS was ≈ 8 J and the volume heated by the arc discharge can be approximated to be ≈ 1.6 mm^3 resulting in an energy density of $w = 5$ J mm^{-3} in the arc (Spahr et al. 2020). With the known size of the precursor dust particles the provided energy per grain in an arc is ≈ 0.04 J. Therefore, it is plausible that the arc discharges provided the required energy Q_{melt} for a complete melting of the dust particles.

We demonstrated that our experimental setup for a chondrule formation experiment aboard the ISS worked as planned. With this experimental setup we were able to obtain dust aggregates with very different sizes and shapes. In contrast to the pristine starting material we observed a strongly reduced porosity of the experimental outcomes. A quantitative interpretation of the porosity may be achieved by small-angle scattering techniques such as SANS (Kahle et al. 2004) in future investigations. With the analyses on eight different aggregates presented here we extended our analysis of micro-structure of the small (∅ ≈ 90 µm) melt droplets by investigations on much bigger and complex shaped fused aggregates with lateral dimensions up to ∅ ≈ 350 µm (Koch et al. 2021b). Our results show that using relatively low discharge energy of 5–8 J, which is much lower than the energies employed in the chondrule formation experiments of e. g. Wdowiak (1996) (5000 J) or Güttler et al. (2008) (123–490 J), leads to the formation of fused aggregates instead of their destruction.

In comparison to our pre-experiments on Earth (Spahr et al. 2020) the fused aggregates obtained aboard the ISS show an increased amount of molten regions which do not only dominate the surface of the Mg_2SiO_4 grains. Molten regions, i. e. reduced porosity, missing grain boundaries and higher density in the contact points of the Mg_2SiO_4 particles reveal that the melting processes aboard the ISS affect also the insides of the aggregates, which was not observed during

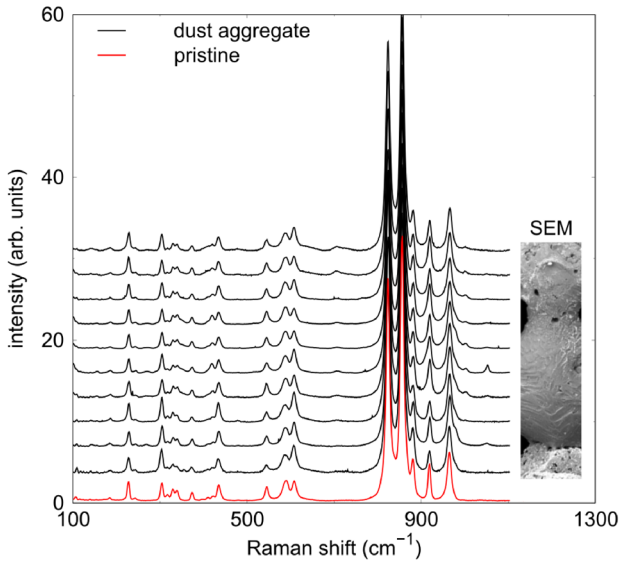

Fig. 7 Raman spectra measured at different points of aggregate #6 in comparison to those of pristine Mg_2SiO_4 dust particles. A section of the corresponding SEM image (Fig. 6b) for the Raman line is shown

the test experiments on Earth. In addition, some parts of the aggregates were molten completely and hence are almost round. This was not observed during the Earth based experiments, were the aggregates only stick together by molten layers covering several Mg_2SiO_4 particles or were fused together by the impact of hot tungsten from the electrodes. It is possible that the aggregates formed aboard the ISS were exposed to more than one discharge while levitating between the electrodes. Therefore, very different morphologies and structures of the aggregates can be observed. This was only possible due to the long-term microgravity conditions aboard the ISS. Here, Mg_2SiO_4 particles and already formed aggregates can be exposed to repeated heating events without suffering from gravity influence. The video recordings obtained from the ISS give evidence that the free levitating dust particles and yet formed aggregates (Fig. 2) are in position between the electrodes and therefore hit by the arc discharges without any contact to the inner walls of the sample chamber, while during the test experiments on Earth these results could not be obtained due to gravitational influences. Implications of the formation of the aggregates for the relation to early Solar System processes are provided by Koch et al. (2022).

In summary, we have obtained further information on the energetics and experimental constraints required for chondrule formation experiments under microgravity conditions aboard the ISS. This provides a roadmap for future experiments on Earth and in microgravity, as it now seems timely and relevant to address the role of the chemical complexity in chondrule formation by lightning experiments by extending the chemical simplicity of the Mg_2SiO_4 model system.

Acknowledgements We gratefully acknowledge the technical help from the HackerSpace FFM e. V., Rainer Haseitl and Solveigh Matthies. The authors are grateful for financial support by the Dr. Rolf M. Schwiete Stiftung, DFG (Wi1232, BA4020), the BMWi (50JR1704), the German Aerospace Center (DLR), ZEISS, BIOVIA, DreamUp, NanoRacks and Nordlicht. We acknowledge DESY (Hamburg, Germany), a member of the Helmholtz Association HGF, for the provision of experimental facilities. Parts of this research were carried out at PETRA III, beamtline P05.

Funding Open Access funding enabled and organized by Projekt DEAL.

References

Asphaug E, Jutzi M, Movshovitz N (2011) Chondrule formation during planetesimal accretion. Earth Planet Sci Lett 308:369–379. https://doi.org/10.1016/j.epsl.2011.06.007

Bayarjargal L, Fruhner CJ, Schrodt N et al (2018) $CaCO_3$ phase diagram studied with Raman spectroscopy at pressures up to 50 GPa and high temperatures and DFT modeling. Phys Earth Planet Inter 281:31–45. https://doi.org/10.1016/j.pepi.2018.05.002

Boss AP (1996) A concise guide to chondrule formation models. In: Hewins RH, Jones RH, Scott ERD (eds) Chondrules and the Protoplanetary Disk, pp 257–263

Bowen NL, Schairer JF (1925) The system MgO-FeO-SiO_3. Am J Sci 29:151–217

Ciesla FJ, Hood LL (2002) The nebular shock wave model for chondrule formation: shock processing in a particle-gas suspension. Icarus 158:281–293. https://doi.org/10.1006/icar.2002.6895

Connolly HC, Jones RH (2016) Chondrules: the canonical and non-canonical views. J Geophys Res-Planets 121:1885–1899. https://doi.org/10.1002/2016JE005113

Connolly HC, Love SG (1998) The formation of chondrules: petrologic tests of the shock wave model. Science 280:62–67. https://doi.org/10.1126/science.280.5360.62

Connolly HC, Jones BD, Hewins RH (1998) The flash melting of chondrules: an experimental investigation into the melting history and physical nature of chondrule precursors. Geochim Cosmochim Acta 62(15):2725–2735. https://doi.org/10.1016/S0016-7037(98)00176-8

Desch SJ, Cuzzi JN (2000) The generation of lightning in the solar nebula. Icarus 143:87–105. https://doi.org/10.1006/icar.1999.6245

Greenwood RC, Herbst W (2021) New constraints on chondrule formation from experimental reproduction of aluminum and titanium in chondrule olivine (abstract # 1617). In: 52nd Lunar and Planetary Science Conference

Güttler C, Poppe T, Wasson JT et al (2008) Exposing metal and silicate charges to electrical discharges: Did chondrules form by nebular lightning? Icarus 195:504–510. https://doi.org/10.1016/j.icarus.2007.11.021

Hewins RH, Fox GE (2004) Chondrule textures and precursor grain size: an experimental study. Geochimica et Cosmochimica Acta 68(4):917–926. https://doi.org/10.1016/S0016-7037(03)00494-0

Hewins RH, Zanda RH, Horanyi M et al (2000) The trouble with flash heating. Lunar Planet Sci 31:1675 (**(abstract)**)

Horányi M, Morfill G, Goertz CK et al (1995) Chondrule formation in lightning discharges. Icarus 114:174–185. https://doi.org/10.1006/icar.1995.1052

Imae N, Isobe H (2017) An experimental study of chondrule formation from chondritic precursors via evaporation and condensation in Knudsen cell: Shock heating model of dust aggregates. Earth Planet Sci Lett 473:256–268. https://doi.org/10.1016/j.epsl.2017.05.040

Johansen A, Okuzumi S (2018) Harvesting the decay energy of ^{26}Al to drive lightning discharge in protoplanetary discs. Astron Astrophys 609:1–22. https://doi.org/10.1051/0004-6361/201630047

Johnson BC, Minton DA, Melosh HJ et al (2015) Impact jetting as the origin of chondrules. Nature 517:339–341. https://doi.org/10.1038/nature14105

Kahle A, Winkler B, Radulescu A et al (2004) Small-angle neutron scattering study of volcanic rocks. Eur J Mineral 16:407–417. https://doi.org/10.1127/0935-1221/2004/0016-0407

Kerr RA (2013) Meteorite mystery edges closer to an answer—or the end of a field. Science 341:126–127. https://doi.org/10.1126/science.341.6142.126

Koch TE, Spahr D, Merges D et al (2021a) Mg_2SiO_4 particle aggregation aboard the ISS—influence of electric fields on aggregation

behavior, particle velocity and shape-preferred orientation. Astron Astrophys 651:A1. https://doi.org/10.1051/0004-6361/202141330
Koch TE, Spahr D, Tkalcec BJ et al (2021b) Formation of chondrule analogs aboard the international space station. Meteorit Planet Sci 56:1669–1684. https://doi.org/10.1111/maps.13731
Koch TE, Spahr D, Tkalcec BJ et al (2022) Formation of fused aggregates under long-term microgravity conditions aboard the iss with implications for early solar system particle aggregation. Meteorit Planet Sci (accepted). https://doi.org/10.1111/maps.13815
Kozub D, Khmelik V, Shapoval J, et al (2018) Helicon Focus 7.0.2 Pro. Helicon Soft Ltd. Available: https://www.heliconsoft.com/heliconsoft-products/helicon-focus/ (2018, Septemper 27)
Krot AN, Amelin Y, Cassen P et al (2005) Young chondrules in CB chondrites from a giant impact in the early Solar System. Nature 436:989–992. https://doi.org/10.1038/nature03830
Libourel G, Portail M (2018) Chondrules as direct thermochemical sensors of solar protoplanetary disk gas. Sci Adv 4:eaar3321. https://doi.org/10.1126/sciadv.aar3321
Lichtenberg T, Golabek GJ, Dullemond CP et al (2018) Impact splash chondrule formation during planetesimal recycling. Icarus 302:27–43. https://doi.org/10.1016/j.icarus.2017.11.004
Limaye A (2012) Drishti: a volume exploration and presentation tool. Proc. SPIE 8506, Developments in X-Ray Tomography VIII, 85060X. https://doi.org/10.1117/12.935640
Lofgren G (1996) A dynamic crystallization model for chondrule melts. In: Hewins RH, Jones RH, Scott ERD (eds) Chondrules and the Protoplanetary Disk, pp 187–196
Moosmann J, Ershov A, Weinhardt V et al (2014) Time-lapse X-ray phase-contrast microtomography for in vivo imaging and analysis of morphogenesis. Nat Protoc 9:294–304. https://doi.org/10.1038/nprot.2014.033
Morlok A, Sutton YC, Braithwaite NSJ et al (2012) Chondrules born in plasma? Simulation of gas-grain interaction using plasma arcs with applications to chondrule and cosmic spherule formation. Meteorit Planet Sci 47:2269–2280. https://doi.org/10.1111/maps.12043
Morris MA, Boley AC (2018) Formation of Chondrules by Shock Waves, vol 1. Cambridge University Press, chap 15:1–17
Navrotsky A, Ziegler D, Oestrike R et al (1989) Calorimetry of silicate melts at 1773 K: measurement of enthalpies of fusion and of mixing in the systems diopside-anorthite-albite and anorthite-forsterite. Contrib Mineral Petrol 101:122–130. https://doi.org/10.1007/BF00387206
Ogurreck M, Wilde F, Herzen J et al (2013) The nanotomography endstation at the PETRA III Imaging Beamline. J Phys Conf Ser 425(18):182002. https://doi.org/10.1088/1742-6596/425/18/182002
Russel S, Connolly HC Jr, Krot AN (eds) (2018) Chondrules: records of protoplanetary disk processes. Cambridge Planetary Science, Cambridge University Press, Cambridge
Russell SS, Connolly HC, Krot AN (eds) (2018) Chondrules: records of protoplanetary disk processes. Cambridge University Press, Cambridge
Spahr D, Koch TE, Merges D, et al (2020) A chondrule formation experiment aboard the ISS: experimental set-up and test experiments. Icarus 350(113):898. https://doi.org/10.1016/j.icarus.2020.113898
Túnyi I, Guba P, Roth LE et al (2003) Electric discharges in the protoplanetary nebula as a source of impulse magnetic fields to promote dust aggregation. Earth Moon Planets 93:65–74. https://doi.org/10.1023/B:MOON.0000034502.21911.22
Wdowiak TJ (1996) Experimental investigation of electrical discharge formation of chondrules. Lunar and Planetary Institute, Houston. In: King EA (ed) Chondrules and their originsk, pp 279–283
Whipple FL (1966) Chondrules: suggestion concerning the origin. Science 153:54–56. https://doi.org/10.1126/science.153.3731.54
Wilde F, Ogurreck M, Greving I et al (2016) Micro-CT at the imaging beamline P05 at PETRA III. AIP Conf Proc 1741(030):035. https://doi.org/10.1063/1.4952858
Wojdyr M (2010) Fityk: a general-purpose peak fitting program. J Appl Cryst 43:1126–1128. https://doi.org/10.1107/S0021889810030499